Journal of Luminescence 280 (2025) 121130

Contents lists available at ScienceDirect

Journal of Luminescence

journal homepage: www.elsevier.com/locate/jlumin

Full Length Article

Spectroscopic evaluation of Ho^{3+}-incorporated alkali and alkaline zinc fluorophosphate glasses: Potential for visible green emission applications

B. Bujji Babu [a,b], S. Vidya Sagar [a,b], K. Venkata Rao [a,*], C. Venkateswarlu [c], N.V. Srihari [d], S.K. Annar [e]

[a] Department of Physics, Government Degree College, Porumamilla, Kadapa, A.P-516193, India
[b] Department of Physics, Yogi Vemana University, Y.S.R, Kadapa -516005, A. P, India
[c] Department of Physics, Jawahar Bharathi Degree College, Kavali-524201, SPSR Nellore, A. P, India
[d] Department of Physics, TRR Government Degree College, Kandukur-523105, Andhra Pradesh, India
[e] Department of Chemistry, DKW(A) Government Degree College, Nellore-524003, A. P, India

ARTICLE INFO

Keywords:
Ho^{3+} ion
JO parameters
Absorption spectra
Emission spectra

ABSTRACT

Alkali and alkaline zinc fluorophosphate (ZFP) glasses doped with Ho^{3+} ions were synthesized and characterized for potential visible green emission applications. The glasses were prepared using the melt-quenching technique with varying concentrations of Ho_2O_3 (0.5, 1.0, 1.5, and 2.0 mol%). The amorphous nature of the glasses was confirmed using X-ray diffraction (XRD) analysis. The presence of functional groups and structural units was determined by Fourier transform infrared (FTIR) spectroscopy and Raman spectroscopy. The optical absorption spectra exhibited ten peaks attributed to transitions from the ground state ($^5I_8$) to various excited states of Ho^{3+}. Judd-Ofelt (JO) intensity parameters (Ω_2, Ω_4, and Ω_6) were evaluated, and the trend $\Omega_2>\Omega_4>\Omega_6$ was observed for all glasses, indicating low symmetry and high covalency around Ho^{3+} ions. The emission spectra obtained under 450 nm excitation, revealed three main peaks corresponding to the $^5F_4\rightarrow{}^5I_8$, $^5F_5\rightarrow{}^5I_8$, and $^5F_4\rightarrow{}^5I_7$ transitions. The $^5F_5\rightarrow{}^5I_8$ transition exhibited the highest branching ratio, stimulated emission cross section, and bandwidth gain among the observed transitions. The $ZFPHo_{0.5}$ glass, containing 0.5 mol% Ho_2O_3, demonstrated the highest branching ratio (96.30 %), stimulated emission cross-section (3.28×10^{-22} cm^2), and bandwidth gain (9.68×10^{-28} cm^3) for the $^5F_5\rightarrow{}^5I_8$ transition, suggesting its suitability for visible laser applications. The decay profiles of the glasses followed a double exponential decay, and the lifetime decreased with increasing Ho^{3+} concentration, owing to concentration quenching. The CIE chromaticity coordinates of the glasses fell within the yellowish-green region, with high colour purity (86.1–87.3 %) and correlated colour temperatures in the range of direct sunlight (4620–4773 K). The results indicate that Ho^{3+}-doped alkali and alkaline zinc fluorophosphate glasses, particularly $ZFPHo_{0.5}$, are promising candidates for visible-green emission applications.

1. Introduction

Rare-earth element-doped glasses are important materials for broadband optical amplifiers, temperature sensors, up-conversion luminescence, solid-state lasers, display devices, and optical fiber technology [1]. In this study, zinc fluorophosphate glasses doped with Ho^{3+} ions were investigated, where the host was phosphate, the network modifier was zinc oxide (ZnO), alkaline oxides such as magnesium oxide (MgO), alkali fluorides such as potassium fluoride (KF) and bismuth trifluoride (BiF_3), and the activator or dopant was holmium oxide (Ho_2O_3). Holmium, a rare earth ion, plays a vital role in laser applications because of its relatively large emission cross-section and metastable energy level [2]. Ho^{3+} ions emit light in several regions, including the blue, green, red, and near-infrared regions, which makes them useful for a variety of purposes, such as radar, visible lasers, and cancer diagnosis [3]. The emission and luminescence decay of the Ho^{3+} ions are noteworthy. When glasses are doped with Ho^{3+} ions, visible green and red emissions generally occur owing to the following transitions: ($^5F_4$,$^5S_2$) $\rightarrow{}^5I_8$ and $^5F_5\rightarrow{}^5I_8$ [4]. The positions and intensities of these emissions depend on the base matrix and concentration of Ho^{3+} ions.

The use of fluoride as a starting material in the production of

* Corresponding author.
E-mail address: drvenkataraok@gmail.com (K. Venkata Rao).

https://doi.org/10.1016/j.jlumin.2025.121130
Received 15 November 2024; Received in revised form 27 January 2025; Accepted 9 February 2025
Available online 10 February 2025

phosphate glasses is crucial for optical applications [5] because it enables the glasses to act as hosts for luminescent rare-earth ions and endows them with the optical properties of fluoride glasses. These glasses also exhibit exceptional mechanical and thermal stabilities. These glasses possess a high level of chemical stability, low melting point, excellent resistance to moisture, relatively low refractive index, and low phonon energy, making them highly transparent in the UV region [6]. Fluorophosphate glasses offer a promising foundation for a wide range of applications in optics, photonics, and energy storage [7]. Ho^{3+} ion-containing fluorophosphate glasses are promising candidates for efficient mid-infrared lasers [8] and green luminescent device applications [9,10].

Recently, there has been considerable academic interest in various glass matrices doped with Ho^{3+} ions owing to their luminescent and laser properties. Recently, Mariselvam et al. (2021) studied a TiO_2–PbO–CaF_2–Li_2CO_3–H_3BO_3 glass system doped with Ho^{3+} ions, focusing on its application in colour displays and optoelectronics [3]. Shoaib et al. (2022) examined the effect of fluoride on the luminescence properties of Ho^{3+} ion-doped BaO-ZnO-Gd_2O_3-P_2O_5 and BaO-ZnO-GdF_3-P_2O_5 glass systems [2]. Baino et al. (2023) explored the potential of Ho^{3+} ions in the SiO_2-CaO-P_2O_5 glass system for 3D scaffold applications [11]. Vani et al. (2023) investigated the structural, thermal, linear, and nonlinear optical properties of a TeO_2+ZnO + BaF_2+$BaCO_3$ glass system doped with Ho^{3+} ions [12]. Pisarska et al. (2023) used the Judd-Ofelt (JO) theory to study a TiO_2-GeO_2-BaO-Ga_2O_3 system doped with Ho^{3+} ions [13]. Naik et al. (2023) investigated the luminescence properties of holmium-doped zinc magnesium lithium fluoroborate (ZMLB) glasses [14]. The present study focuses mainly on the evaluation of zinc fluorophosphate glasses doped with Ho^{3+} ions for potential use in solid-state visible laser applications. A thorough investigation was conducted, which included a detailed examination of optical absorption using Judd-Ofelt analysis, as well as profiles of emission, decay, and colour characteristics.

2. Experimental

2.1. Glass preparation

The current study utilized a conventional method, melt quenching, to fabricate ZFP glasses with various concentrations of Ho^{3+} ions. High-grade chemicals with a purity of 99.99 %, including Himedia $NH_4H_2PO_4$, KF, MgO, ZnO, Ho_2O_3, and Otto's BiF_3, were used according to the empirical formula (60-x) P_2O_5+10MgO+10ZnO+10BiF_3+10 KF + xHo_2O_3, with x values of 0.5, 1.0, 1.5, and 2.0 mol%. The compositions of the glass systems and their codes are presented in Table 1.

The chemicals were mixed in a stoichiometric ratio and ground using an agate mortar to ensure their homogeneity. The mixture was then placed in an aluminium crucible and heated in an electric heating chamber at 1150 °C for 1 h. Subsequently, the molten substance was quenched on a brass plate and pressed through another brass plate. To minimize internal stress, the resulting transparent glasses were placed in an electric heating chamber and annealed at 400 °C for 3 h. Finally, the glass was cooled to room temperature after annealing.

Table 1
Nominal compositions of the prepared glass system with respective codes.

Glass code	Composition (mol %)					
	MgO	ZnO	KF	BiF_3	P_2O_5	Ho_2O_3
$ZFPHo_{0.5}$	10	10	10	10	59.5	0.5
$ZFPHo_{1.0}$	10	10	10	10	59.0	1.0
$ZFPHo_{1.5}$	10	10	10	10	58.5	1.5
$ZFPHo_{2.0}$	10	10	10	10	58.0	2.0

2.2. Characterization

The refractive indices (n) of the Ho^{3+} ion-doped ZFP glass were precisely determined at room temperature using an Abbe ATAGO refractometer operating at a yellow sodium D spectral line of 589 nm with 1-bromonaphthalene serving as the contact liquid. The densities of the synthesized Ho^{3+}-ion-doped alkali and alkaline ZFP glasses were determined at room temperature using a Shimadzu digital weighing balance and Archimedes' principle, with deionized water serving as the immersion liquid. The amorphous nature of Ho^{3+}-ion-doped alkali and alkaline ZFP glasses was characterized using a Rigaku Mini Flex 600 X-ray diffractometer with Cuα radiation. A JSM-IT 500 MODEL manufactured by JEOL, equipped with a remarkable AMETEK EDS device, was used to capture the SEM images. The KBr pellet technique was employed to acquire FTIR spectra in the 4000-500 cm^{-1} range via a Bruker Alpha Compact FTIR spectrophotometer. An Invia Reflex Laser Confocal Raman Microscope with a spectrometer (Renishaw Metrological Systems UK) was used to acquire the Raman spectrum, which ranged from 100 cm^{-1} to 1500 cm^{-1}. A JASCO V570 spectrophotometer with a resolution of 1.0 nm was used to record the optical absorption spectra in the UV–Vis–NIR region at room temperature. A JOBIN YVON Fluorolog-3 fluorometer equipped with a double-beam monochromator in front-surface mode (22.5°) and a 450 W xenon lamp as the excitation source was used to measure the excitation and emission spectra and decay profiles of alkali and alkaline ZFP glasses doped with Ho^{3+} ions at all concentrations in the visible region.

3. Results and discussion

3.1. Physical properties

At room temperature, the n values of alkali and alkaline ZFP glasses doped with Ho^{3+} were evaluated at various concentrations (0.5, 1.0, 1.5, and 2.0 mol%), and the observed values were 1.651, 1.652, 1.654, and 1.655, respectively. Density (ρ) exhibited a positive linear relationship with the quantity of holmium. In particular, the density (ρ) values of Ho^{3+} ions doped at 0.5, 1.0, 1.5, and 2.0 mol% ZFP glasses were 3.249, 3.592, 3.759, and 4.001 gm/cm^3, respectively. These findings suggest that the concentration of holmium ions directly affects the enhancement of both refractive indices and density values. Other physical parameters were calculated via density (ρ) and refractive index (n) using equations explained elsewhere in the literature [15]. The results are presented in Table 2. As shown in Fig. 1, as the concentration of Ho^{3+} ions increased, the molar volume (V_m) of the alkali and alkaline ZFP glasses decreased from 56.431 to 46.378 cm^3 mol^{-1}, the molar refraction (R_m) values decreased from 20.608 cm^3 to 17.019 cm^3, the electronic polarizability

Table 2
Important physical and optical parameters.

Parameter	$ZFPHo_{0.5}$	$ZFPHo_{1.0}$	$ZFPHo_{1.5}$	$ZFPHo_{2.0}$
Refractive Index, n	1.651	1.652	1.654	1.655
Thickness t (cm)	0.265	0.325	0.375	0.285
Density, ρ (gm/cm^3)	3.249	3.592	3.759	4.001
Average Molecular Weight (gm/mol)	183.34	184.08	184.82	185.56
Concentration, N × 10^{22} (ions/cm^3)	0.534	1.175	1.837	2.597
Molar Volume, V_m ($cm^3.mol^{-1}$)	56.431	51.248	49.168	46.378
Molar Refraction, R_m (cm^3)	20.608	18.738	18.021	17.019
Transmission Coefficient T	0.886	0.886	0.886	0.885
Reflection Loss, R_L (%)	6.030	6.044	6.072	6.086
Molar electronic polarizability, α_m ($10^{-24}.cm^3$)	8.178	7.436	7.151	6.754
Dielectric Constant ε	2.726	2.729	2.736	2.739
Optical Dielectric Constant ε_{opt}	1.726	1.729	1.736	1.739
Metallization factor (m)	0.635	0.634	0.633	0.633
Inter ionic distance R_i (Å)	1.233	0.948	0.816	0.728
Polaran Radius R_P (Å)	0.789	0.606	0.522	0.465

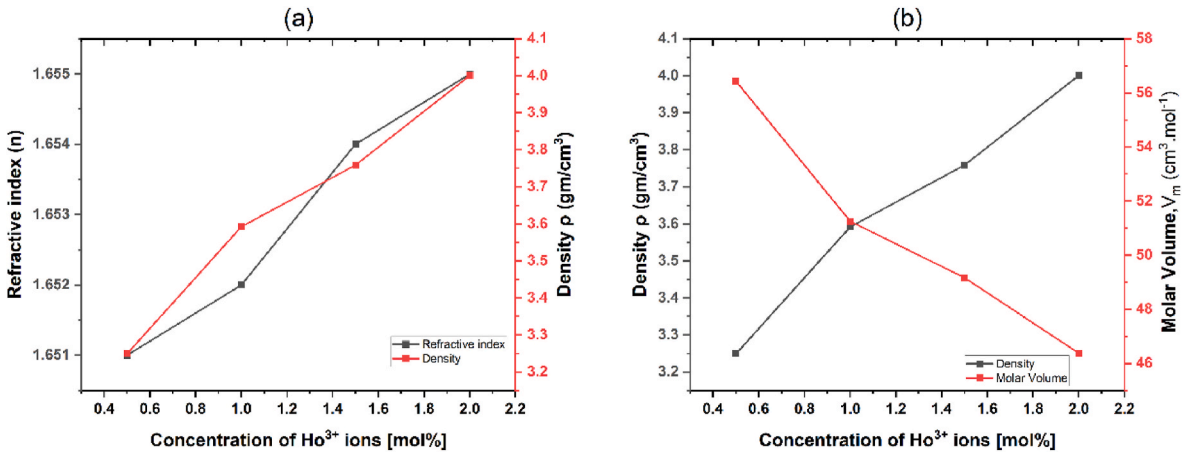

Fig. 1. Variation of properties with respect to concentration of Ho^{3+} ions a) Refractive index vs Density b) Density vs Molar volume.

(α_m) decreased from 8.178 cm^3 to 6.754 cm^3, and the interionic distance and polaron radius decreased from 1.233 to 0.728 Å and 0.789 Å to 0.465 Å, respectively. The reflection loss, dielectric constant, and optical dielectric constant increased from 6.030 % to 6.086 %, 2.726 to 2.739, and 1.726 to 1.739, respectively. Density and molar volume are useful for predicting structural changes in glass matrices [16]. This increase in density may be due to the replacement of the less dense oxides (P_2O_5) with denser oxides (Ho_2O_3). A decrease in molar volume indicates a change in the structure of the vitreous network as a function of composition [17]. The calculated metallization factor (M) values indicate that $R_m/V_m < 1$, which indicates that the prepared glasses are amorphous in nature and supports the XRD results [18].

3.2. XRD analysis

X-ray diffraction (XRD) patterns are shown in Fig. 2, revealing the characteristics of alkali and alkaline ZFP glasses doped with Ho^{3+}. After inspection, no peaks were observed, indicating the presence of crystals. Instead, a wide hump, which is characteristic of amorphization, is observed in the 10–40° range. Thus, the XRD profiles show that the glass samples under investigation maintained their amorphous nature.

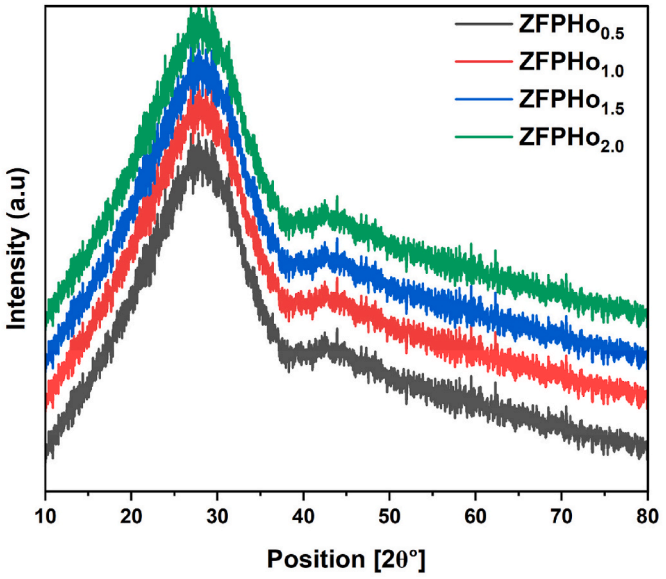

Fig. 2. X-ray diffraction profiles of ZFP glasses doped with different concentrations of Ho^{3+} ions.

3.3. Morphological studies

Fig. 3 shows the EDX spectrum of a typical $ZFPHo_{2.0}$ glass sample. The peaks in Fig. 3 represent the distinctive X-rays of P, O, F, Zn, Ho, K, Mg, and Bi, which are evenly distributed across the observation region. Significant intensities were observed among the peaks at approximately 0.5 keV and 2.0 keV, which correspond to phosphorus and oxygen, respectively. This spectrum indicates the presence of components in the analyzed glass samples. The surface morphologies of alkali and alkaline ZFP glasses doped with 2.0 mol% Ho^{3+} ions were captured by scanning electron microscopy (SEM), as shown in the inset of Fig. 3. The inset of the morphological image in Fig. 3 shows the surface morphology of the glass sample, revealing that there were no crystals or flaws on the surface. SEM and EDS confirmed that the prepared glass samples were amorphous and that all the elements were present.

3.4. Vibrational studies (FTIR and Raman spectroscopy)

The presence of functional groups and configurations of different structural units in the synthesized glasses were determined by Fourier transform infrared (FTIR) spectroscopy [19]. Vibrations related to structural units are thought to be independent of those generated by nearby units [20]. Fig. 4 shows the FTIR spectra of alkali and alkaline ZFP glasses doped with different concentrations of Ho^{3+} ions. One can perceive eleven IR bands at 539, 726, 902, 1077, 1269, 1479, 1595,

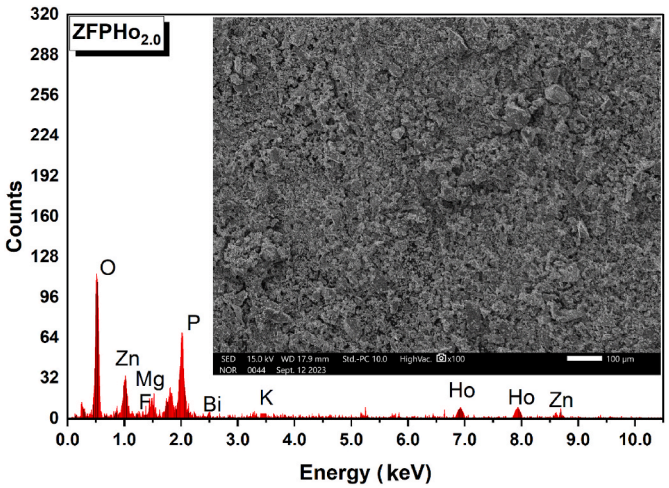

Fig. 3. Representative image of surface morphology and EDX spectrum of ZFP glasses doped with 2.0 mol% of Ho^{3+} ions.

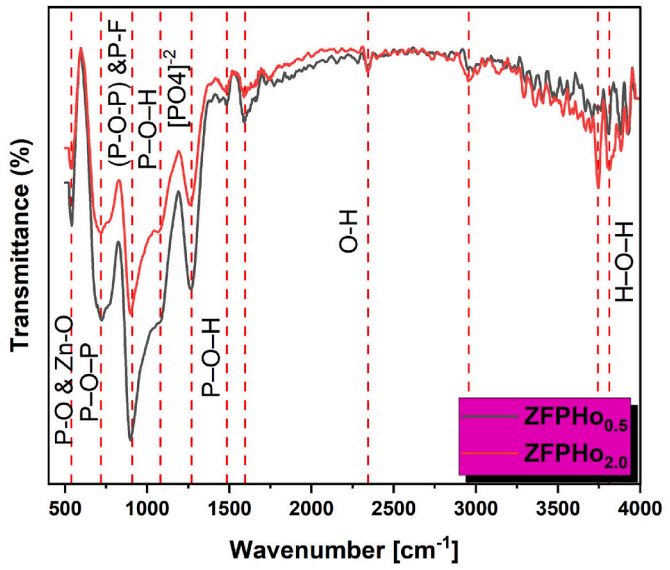

Fig. 4. Fourier transform IR spectra of ZFP glasses doped with 0.5 and 2.0 mol % of Ho^{3+} ions.

2343, 2956, 3750 and 3810 cm^{-1}, which are in the range of 4000-500 cm^{-1}. Among the 11 bands, five were in the functional group region and the remaining six were in the fingerprint region. The P-O bond stretching vibrations with Zn-O vibrations are responsible for the band at 539 cm^{-1} [21]. The band at 726 cm^{-1} is attributed to P–O–P bond symmetric stretching vibrations [9]. The symmetric stretching of the ν_{sy}(P-O-P) molecule with P-F groups and a linear metaphosphate chain is indicated by the band at 902 cm^{-1} [22]. The P–O and P–O–H stretching vibrations are represented by bands at 1077 cm^{-1} and 1479 cm^{-1}, respectively [23]. The asymmetric stretching vibrations of tetrahedral $[PO_4]^{3-}$ units linked to two nonbridging oxygen atoms (NBOs) are responsible for the peak at 1269 cm^{-1} [24]. The asymmetric stretching vibrations of the O–H bond are responsible for the vibrational band at 2343 cm^{-1} [25]. Owing to the presence of NBOs in phosphate, the H–O–H stretching vibrations of hydroxyl groups are responsible for the peaks at approximately 3755 and 3810 cm^{-1} [26]. As the concentration of Ho^{3+} increased (Fig. 4), only the band intensities changed, leaving the total number of bands unchanged.

The Raman spectrum of the $ZFPHo_{1.5}$ glass sample is shown in Fig. 5.

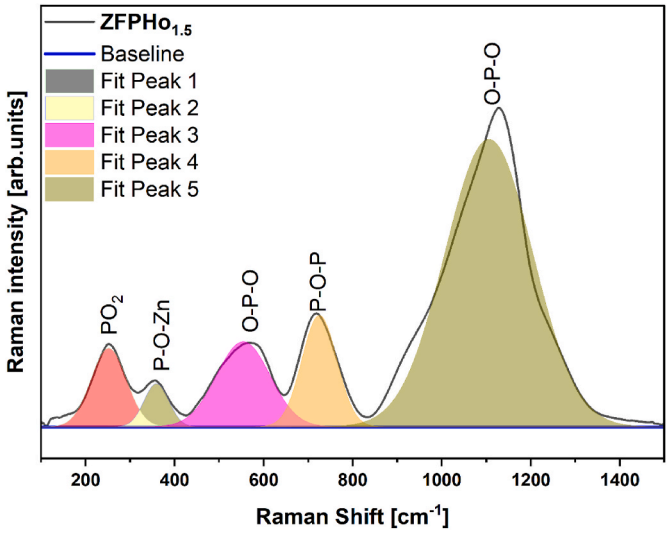

Fig. 5. Deconvoluted Raman spectrum of ZFP glass doped with 1.5 mol% Ho^{3+} ions.

Five Raman bands were identified in the studied glass, with Raman shifts of 258, 340, 575, 702, and 1139 cm^{-1}. The band at 1139 cm^{-1} displayed the highest intensity among the five bands and was attributed to the symmetric stretching vibration of the O-P-O groups in the Q^2 tetrahedra of the metaphosphate glass [27]. The remaining Raman bands were attributed to the weak vibrations caused by PO_2 bending (258 cm^{-1}) [27], P-O-Zn chain bending (340 cm^{-1}) [28], O-P-O tetrahedral PO_4^{3-} bending (575 cm^{-1}) [29], and P-O-P bridge oxygen stretching (702 cm^{-1}) [30]. The Raman spectra suggest that the prepared alkali and alkaline zinc fluorophosphate glasses were constructed using phosphate and different network modifiers, as identified by FTIR.

3.5. Analysis of the optical absorption spectra and oscillator strengths

The optical absorption spectra of the Ho^{3+}-ion-doped alkali and alkaline ZFP glasses were observed in the UV–visible region, as shown in Fig. 6. Ten peaks are observed. According to Carnall [31], these peaks are attributed to transitions of Ho^{3+} ions from the ground state $^5I_8$ to different excited states, $^5F_5$, $^5F_4$, $^5F_3$, $^5F_2$, $^5F_1$, $(^5G, ^3G)_5$, $^5G_4$, $^3H_6$, $^3L_9$, and $^3K_6$, at wavenumbers of ~15612, ~18635, ~20612, ~21271, ~22418, ~24003, ~25980, ~27782, ~29054, and ~30054 cm^{-1}, respectively. The $^5I_8 \rightarrow {}^5F_1$ transition occurring at approximately 22,218 cm^{-1} is more intense than the other transitions and is sensitive to changes surrounding the Ho^{3+} ions, and adheres to the selection criteria of $2 \geq |\Delta L|$, $\Delta S = 0$, and $2 \geq |\Delta J|$ [3]. Hence, the $^5I_8 \rightarrow {}^5F_1$ transition is referred to as the hypersensitive transition (HST). Using the most well-known theory proposed by prominent scientists B. R. Judd [32] and G. S. Ofelt [33], called the Judd-Ofelt theory, calculated oscillator strengths for the different transitions found in the absorption spectra of alkali and alkaline ZFP glasses containing Ho^{3+} ions. The probability of transitions between the energy levels in atoms or molecules is measured by oscillator strength, a dimensionless quantity [1]. There are two types of oscillator strengths: experimental (f_{exp}) and theoretical (f_{cal}) [34]. According to JO theory [35], both the experimental (f_{exp}) and theoretical (f_{cal}) oscillator strengths were calculated using the following equations:

$$f_{exp} = 4.319 \times 10^{-9} \int \varepsilon(\bar{\vartheta}) d\bar{\vartheta} \quad (1)$$

where $\varepsilon(\bar{\vartheta})$ is the molar extinction coefficient.

$$f_{cal} = \frac{8\pi^2 mc\nu}{3he^2(2j+1)} \times \frac{(n^2+2)^2}{9n} \sum_{\lambda=2,4,6} \Omega_\lambda \langle \psi j \parallel U^\lambda \parallel \psi J' \rangle^2 \quad (2)$$

where h, e, and m are the Planck's constant, charge, and mass of an electron, respectively. Where $\sum_{\lambda=2,4,6} \Omega_\lambda \langle \psi j \parallel U^\lambda \parallel \psi J' \rangle^2$ is the line

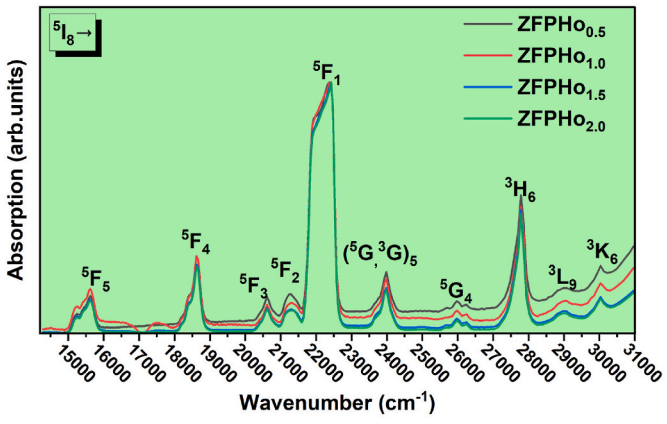

Fig. 6. Optical absorption spectra of ZFP glasses doped with different concentrations of Ho^{3+} ions in the UV–Visible region.

strength, n is the refractive index, and Ω_λ represents the JO parameter. The results are presented in Table 3. Table 3 shows that the oscillator strengths (f_{exp} and f_{cal}) of the $^5I_8 \rightarrow {}^5F_1$ transition occurred at a wavenumber of 22,218 cm^{-1}, which is noteworthy for all the fabricated alkali and alkaline ZFP glasses. Among the prepared alkali and alkaline ZFP glasses, glasses doped with 0.5 mol% Ho^{3+} ($ZFPHo_{0.5}$) presented the highest oscillator strengths (f_{exp}, and f_{cal}). This indicates that the $ZFPHo_{0.5}$ glass exhibits the highest radiative transition probabilities. To evaluate the quality of fit between the experimental (f_{exp}) and theoretical (f_{cal}) oscillator strengths, the root-mean-square deviation (δ_{RMS}) was calculated using the following equation [36]:

$$\delta_{RMS} = \sqrt[2]{\frac{\sum \left(f_{exp} - f_{cal}\right)^2}{N}} \quad (3)$$

where N is the number of transitions used in the fit. The obtained δ_{RMS} values were very low (0.63×10^{-6}, 0.18×10^{-6}, 0.13×10^{-6}, and 0.11×10^{-6}) for the studied alkali and alkaline ZFP glasses doped with Ho^{3+} ions. These low δ_{RMS} values demonstrate a good fit between the theoretical and experimental (f_{exp} and f_{cal}) oscillator strengths, and confirm the accuracy of the JO intensity parameters [37].

3.6. Analysis of Judd-Ofelt (JO) and radiative parameters

A deeper understanding of the nearby framework encompassing rare-earth ions via an analysis of the JO intensity parameters Ω_λ (where $\lambda = 2,4$, and 6) is feasible. The Ω_2 value generally characterizes the degree of asymmetry and covalency between the RE ions and local ligand anions, whereas the Ω_4 and Ω_6 values reflect the bulk properties of the medium, such as rigidity and viscosity [4]. The Ω_2 value is strongly influenced by hypersensitive transitions in the absorption spectra [38]. The JO intensity parameters Ω_λ ($\lambda = 2,4,6$) of the alkali and alkaline ZFP glasses doped with Ho^{3+} ions were computed using the following equation [39], $\Omega_\lambda = 9.22 \times 10^{-12} \left[\frac{9n(2J+1)}{(n^2+2)^2}\right] \times T_\lambda$ (4)

where n and J denote the refractive index and ground state, respectively, and T_λ represents the product of the total reduced matrix elements and the overall experimental oscillator strength. Table 4 presents the Judd-Ofelt intensity parameters for the studied alkali and alkaline ZFP glasses, along with those of other Ho^{3+}-doped glasses from previous reports. In the present study, the JO intensity parameters of all studied alkali and alkaline ZFP glasses exhibited a consistent trend of $\Omega_2 > \Omega_4 > \Omega_6$. Each glass system has distinctive intensity parameters, covalence, and asymmetry factors; however, the Ho^{3+} ion-infused glass systems, including LaF_3 [40], fluoride [41], LBTAFHo10 [42], BaPbAlFBHo0.5 [28], GdCaSBHo10 [3], and AYFT [43], followed the same trend. It is evident from the present study that the Ω_2 parameter magnitudes are larger than those of the Ω_4 and Ω_6 parameters, confirming the low symmetry and high covalency of Ho^{3+} ions in the prepared alkali and alkaline ZFP glasses. The JO parameters exhibited variations in relation to the glass composition, following the descending order of $ZFPHo_{0.5} > ZFPHo_{1.0} > ZFPHo_{2.0} > ZFPHo_{1.5}$. The JO parameters decreased as the concentration of Ho3 + ions increased from 0.5 to 1.5 mol%. However, upon further increasing the concentration of Ho^{3+} ions, the JO parameter increased. As the Ho^{3+} ion concentration increased from 0.5 to 1.5 mol%, the magnitude of Ω_2 decreased, indicating a reduction in the asymmetry and covalency of the Ho-O bond [20]. However, beyond 1.5 mol%, the Ω_2 value increases with increasing Ho^{3+} ion concentration, suggesting an increase in the asymmetry and covalency of the Ho-O bond due to the cross-relaxation process. Glass $ZFPHo_{0.5}$ has significant JO parameters, specifically Ω_2 (1.38×10^{-20}), Ω_4 (0.56×10^{-20}) and Ω_6 (0.55×10^{-20}), indicating exceptional quality. The quality factor (χ), which can be used to predict the stimulated emission of laser materials, is the ratio of Ω_4 to Ω_6 [13]. These values were calculated for all the studied Ho^{3+}-doped alkali and alkaline ZFP glasses, and the results are presented in Table 4. As shown in Table 4, the quality factor (χ) values were in the range of 1.0–1.80. The obtained higher value of the spectroscopic quality factor is beneficial for lasing applications [44].

Using the J-O intensity parameters and refractive indices (n), radiative properties such as the radiative total transition probabilities (A_T) and radiative lifetimes (τ_R) of $^3H_5$, $^5G_6$, $^3K_8$, $^5F_2$, $^5F_3$, $^5F_4$, and $^5F_5$ excited levels of the studied alkali and alkaline ZFP glasses doped with different concentrations of Ho^{3+} ions were calculated. Table 5 presents the results of this study. The magnitudes of the total radiative transition probabilities (A_T) were in the order $^5G_6 > {}^3H_5 > {}^5F_4 > {}^5F_3 > {}^5F_5 > {}^5F_2 > {}^3K_8$ for all the studied ZFP glasses. Among the four prepared alkali and alkaline ZFP glasses, the $ZFPHo_{0.5}$ glass had the highest magnitude of total transition probability (A_T) compared to the remaining studied glasses at all levels. The magnitude of the A_T for the $ZFPHo_{0.5}$ glass was 8535 s^{-1} for the $^5G_6$ level. The radiative lifetime (τ_R) is the inverse of the total transition probability (A_T). The radiative lifetime (τ_R) values were calculated for all levels of the Ho^{3+}-doped alkali and alkaline ZFP glasses. In this study, the $^3K_8$ level had the highest magnitude of radiative lifetime (τ_R) among all the levels. The magnitudes of the radiative lifetimes (τ_R) were in the order of $^5G_6 < {}^3H_5 < {}^5F_4 < {}^5F_3 < {}^5F_5 < {}^5F_2 < {}^3K_8$ for all glasses. Among the studied glasses, the $ZFPHo_{2.0}$ glasses had the highest radiative lifetime of 10707 μs for the $^3K_8$ level.

3.7. Photoluminescence analysis

The excitation spectra of various concentrations of Ho^{3+}-doped alkali and alkaline ZFP glasses were recorded at room temperature in the range 350–500 nm. These spectra were identical to the excitation

Table 3
Experimental and calculated oscillator strengths (f_{exp}, $f_{cal} \times 10^{-6}$) of certain excited states and root mean square deviations ($\delta_{RMS} \times 10^{-6}$) of studied ZFP glasses doped with different concentration of Ho^{3+} ions.

Transition $^5I_8 \rightarrow$	$ZFPHo_{0.5}$		$ZFPHo_{1.0}$		$ZFPHo_{1.5}$		$ZFPHo_{2.0}$	
	f_{exp}	f_{cal}	f_{exp}	f_{cal}	f_{exp}	f_{cal}	f_{exp}	f_{cal}
$^5F_5$	0.55	0.82	0.33	0.36	0.15	0.21	0.14	0.20
$^5F_4$	0.92	0.93	0.39	0.40	0.23	0.22	0.22	0.21
$^5F_3$	0.49	0.37	0.15	0.16	0.09	0.08	0.08	0.07
$^5F_2$	0.58	0.21	0.20	0.09	0.11	0.05	0.10	0.04
$^5F_1+{}^5G_8$	5.48	5.58	2.38	2.42	1.66	1.69	1.99	2.00
$(^5G, {}^3G)_5$	1.00	0.68	0.36	0.31	0.26	0.21	0.27	0.22
$^5G_4$	0.56	0.09	0.16	0.04	0.14	0.02	0.16	0.02
$^3H_6$	1.71	0.95	0.70	0.41	0.48	0.29	0.44	0.35
$^3L_9$	1.19	0.31	0.29	0.13	0.22	0.07	0.20	0.07
$^3K_6$	1.44	0.01	0.44	0.01	0.29	0.00	0.27	0.00
δ_{RMS}	±0.63		±0.18		±0.13		±0.11	

Table 4
JO intensity parameters (Ω_2, Ω_4, $\Omega_6 \times 10^{-20}$ cm^2), trends and spectroscopic quality factor(χ) of studied ZFP glasses along with other glasses doped with Ho^{3+} ions.

Glass code	Ω_2	Ω_4	Ω_6	Trend	Quality factor (χ)
$ZFPHo_{0.5}$[Present work]	1.38	0.56	0.55	$\Omega_2>\Omega_4>\Omega_6$	1.00
$ZFPHo_{1.0}$[Present work]	0.59	0.26	0.24	$\Omega_2>\Omega_4>\Omega_6$	1.08
$ZFPHo_{1.5}$[Present work]	0.42	0.17	0.12	$\Omega_2>\Omega_4>\Omega_6$	1.41
$ZFPHo_{2.0}$[Present work]	0.51	0.18	0.10	$\Omega_2>\Omega_4>\Omega_6$	1.80
LaF_3 [40]	1.03	0.98	0.31	$\Omega_2>\Omega_4>\Omega_6$	3.16
Fluoride [41]	2.78	1.39	1.23	$\Omega_2>\Omega_4>\Omega_6$	1.13
LBTAFHo10 [42]	2.74	2.35	1.72	$\Omega_2>\Omega_4>\Omega_6$	1.37
BaPbAlFBHo0.5 [28]	2.98	2.92	1.35	$\Omega_2>\Omega_4>\Omega_6$	2.16
GdCaSBHo10 [3]	2.84	2.11	1.18	$\Omega_2>\Omega_4>\Omega_6$	1.79
AYFT [43]	1.68	1.64	0.89	$\Omega_2>\Omega_4>\Omega_6$	1.84

Table 5
Radiative total transition probabilities (A_T, s^{-1}), and radiative lifetimes (τ_R, μs) of certain excited states of studied ZFP glasses doped with different concentration of Ho^{3+} ions.

Glass code	$^3H_5$		$^5G_6$		$^3K_8$		$^5F_2$		$^5F_3$		$^5F_4$		$^5F_5$	
	A_T	τ_R	A_T	τ_R	A_T	τ_R	A_T	τ_R	A_T	τ_R	A_T	τ_R	A_T	τ_R
$ZFPHo_{0.5}$	5160	194	8535	117	394	2541	510	1960	880	1136	1120	893	746	1341
$ZFPHo_{1.0}$	2248	445	3719	269	171	5851	222	4513	385	2598	494	2026	331	3020
$ZFPHo_{1.5}$	1515	660	2570	389	97	10309	117	8547	208	4803	274	3647	189	5288
$ZFPHo_{2.0}$	1735	576	3007	333	93	10707	103	9756	188	5325	254	3943	180	5556

spectra of 0.5 mol% Ho^{3+}-doped alkali and alkaline ZFP glass, as shown in Fig. 7. As shown in Fig. 7, the spectra exhibited six peaks at wavelengths of 362, 373, 418, 450, 473, and 487 nm. These peaks were due to transitions from the ground state $^5I_8$ to different excited states $^3H_6$, $^5G_4$, $(^5G,^3G)_5$, $^5F_1$, $^5F_2$, and $^5F_3$. Among the six peaks, the peak at 450 nm is significantly more intense than the other peaks. This indicates that the $^5I_8 \rightarrow {}^5F_1$ transition at 450 nm can effectively serve as an excitation source for capturing the emission spectra of the fabricated alkali and alkaline ZFP glass samples.

The emission spectra of the Ho^{3+} ion-doped alkali and alkaline ZFP glasses, when excited at 450 nm in the UV–vis region, are displayed in Fig. 8. Three main peaks were observed in the emission spectra, which were assigned to the $^5F_4 \rightarrow {}^5I_8$, $^5F_5 \rightarrow {}^5I_8$, and $^5F_4 \rightarrow {}^5I_7$ transitions, corresponding to wavelengths of ~538, ~679, and ~764 nm, respectively [45]. The figure shows that Among the three peaks, the peak at 679 nm had the highest intensity. One of the most important parameters in laser physics and optical engineering is the stimulated emission cross-section (σ_P), which is considered when analysing laser characteristics. Another important factor in laser design is the branching ratio [46]. The suitability of a material for laser applications depends critically on its stimulated emission cross-section (σ_P), branching ratio (β_{exp}), and bandwidth gain (BWG) values [2]. To select materials for lasing applications, materials with branching ratios equivalent to or greater than 50 % are required to yield better laser action [47]. Among the three transitions, the $^5F_5 \rightarrow {}^5I_8$ transition resulted in the highest branching ratio. Among the prepared glasses, the $ZFPHo_{0.5}$ glass had the highest branching ratio (β_{exp}) of 96.30 % for the $^5F_5 \rightarrow {}^5I_8$ transition. Stimulated emission cross-sections (σ_P) were calculated using the following Füchtbauer –Ladenburg equation [48,49]:

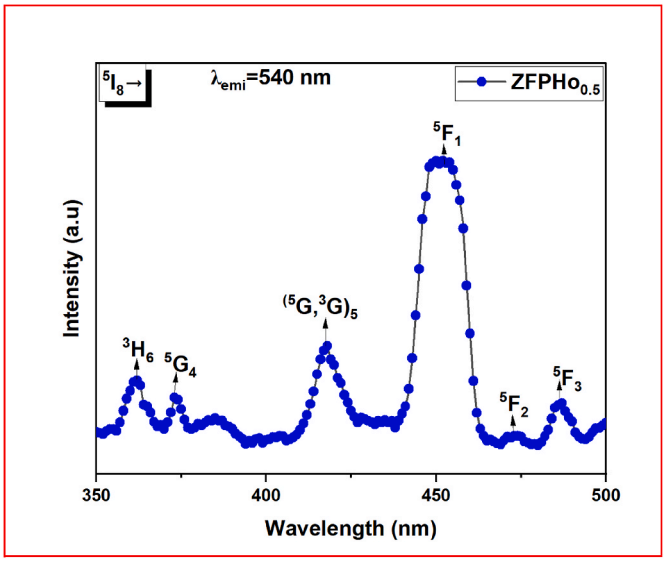

Fig. 7. Representative excitation spectrum of 0.5 mol% Ho^{3+} ions doped ZFP glass sample.

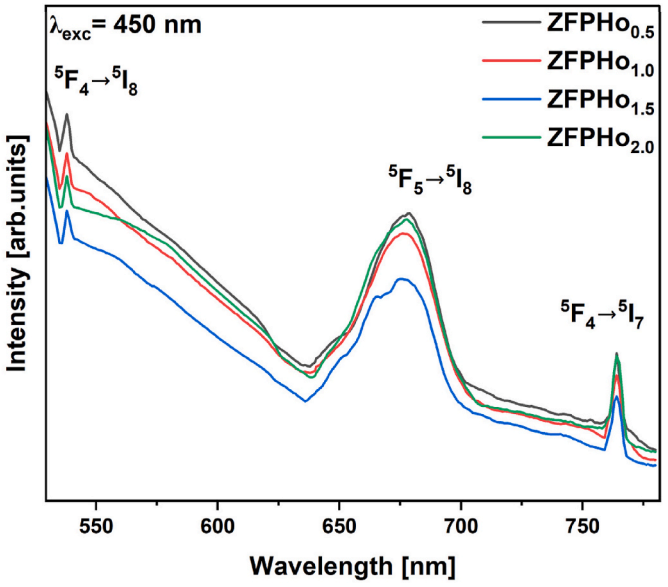

Fig. 8. Emission spectra of ZFP glass doped with different concentrations of Ho^{3+} ions at stimulated wavelength of 450 nm.

$$\sigma_P = \frac{\lambda_p^4 \times A_R}{8\pi c n^2 \times \Delta\lambda_{eff}} \quad (5)$$

where λ_P, A_R, and $\Delta\lambda_{eff}$ are the wavelength of the peak stimulated emission, the transition probability rate, and the effective bandwidth of the transition, respectively. The bandwidth (BWG) gains were calculated from the obtained stimulated emission cross-section (σ_p) values and the effective bandwidths ($\Delta\lambda_{eff}$). Bandwidth gain is the product of the stimulated emission cross-section (σ_P) and effective bandwidth ($\Delta\lambda_{eff}$) of the transition [50] and is an important laser parameter for identifying lasing in glass hosts and near-infrared broadband amplification [51]. Table 6 presents the results. As shown in Table 6, the $^5F_5 \rightarrow {}^5I_8$ transition displayed higher values of experimental branching ratios (β_{exp}, %), stimulated emission cross-sections ($\sigma_p \times 10^{-22}$ cm^2), and bandwidth gains ($\sigma_p \times \Delta\lambda_{eff}$) among the three observed transitions. Upon increasing the concentration of Ho^{3+} ions, the stimulated emission cross-section (σ_P) decreased. Typically, transitions with a higher value of the emission cross-section (σ_P) demonstrate high-gain and low-threshold laser operation [52]. For the prepared glasses, among the three transitions, the $^5F_5 \rightarrow {}^5I_8$ transition resulted in high magnitudes of stimulated emission cross sections (σ_P) and bandwidth gain ($\sigma_p \times \Delta\lambda_{eff}$) values of 3.28 × 10^{-22} cm^2, and 9.68 × 10^{-28} cm^3, respectively. Among the four fabricated alkali and alkaline ZFP glasses, the $ZFPHo_{0.5}$ glass had elevated values of β_{exp}, σ_P, and $\sigma_p \times \Delta\lambda_{eff}$ compared with those of the other glasses. Based on the results obtained, it can be inferred that $ZFPHo_{0.5}$ glass has potential as a suitable contender for visible-laser applications.

Ho^{3+} ion-doped alkali and alkaline ZFP glasses were stimulated at a wavelength of 450 nm, and their emission spectra were subsequently

Table 6
Peak emission wavelength ($\lambda_{P,\ nm}$), radiative transition probability (A_R, s^{-1}), experimental branching ratios ($\beta_{exp,}$ %), stimulated emission cross-section ($\sigma_p \times 10^{-22}$, cm^2), and bandwidth gain ($\sigma_p \times \Delta\lambda, \times 10^{-28}$, cm^3) of studied ZFP glasses doped with different concentration of Ho^{3+} ions for the $^5F_4 \rightarrow {}^5I_8$, $^5F_5 \rightarrow {}^5I_8$, and $^5F_4 \rightarrow {}^5I_7$ transitions.

Glass code	Transition	λ_P	A_R	β_{exp} (%)	$\sigma_p \times 10^{-22}$	$\sigma_p \times \Delta\lambda \times 10^{-28}$
$ZFPHo_{0.5}$						
	$^5F_4 \rightarrow {}^5I_8$	538	921.5	1.76	0.36	0.10
	$^5F_5 \rightarrow {}^5I_8$	679	569.2	96.30	3.28	9.68
	$^5F_4 \rightarrow {}^5I_7$	764	84.6	5.58	0.08	0.02
$ZFPHo_{1.0}$						
	$^5F_4 \rightarrow {}^5I_8$	538	404	1.35	0.14	0.03
	$^5F_5 \rightarrow {}^5I_8$	678	253.1	93.20	1.57	5.03
	$^5F_4 \rightarrow {}^5I_7$	764	38.9	5.45	0.05	0.02
$ZFPHo_{1.5}$						
	$^5F_4 \rightarrow {}^5I_8$	538	219.6	1.28	0.07	0.02
	$^5F_5 \rightarrow {}^5I_8$	676	144.4	82.37	0.92	3.05
	$^5F_4 \rightarrow {}^5I_7$	764	24.8	4.52	0.03	0.01
$ZFPHo_{2.0}$						
	$^5F_4 \rightarrow {}^5I_8$	538	199.3	1.28	0.06	0.01
	$^5F_5 \rightarrow {}^5I_8$	678	137.1	92.43	0.87	2.84
	$^5F_4 \rightarrow {}^5I_7$	764	25.7	6.29	0.03	0.01

utilized to determine the color coordinates, which are illustrated in the 1931 CIE color chart shown in Fig. 9, and the values are presented in Table 7. These color coordinates fall within the yellowish–green region and are situated near the locus line. The CCT values were computed using the following equation of McCamy's approximation [53], the correlated colour temperatures (CCTs) were computed.

$$CCT = 437n^3 + 3601n^2 + 6861n + 5517 \quad (6)$$

n is the reciprocal slope calculated using the equation, $n = (x - 0.332)/(y - 0.186)$, where x and y are the chromaticity co-ordinates. The color purity and dominant wavelengths were calculated using Osram color calculator software, and the results are presented in Table 7. The calculated CCT values ranged from 4620 K to 4773 K, falling within the range of direct sunlight (4500–5000 K). The color purities were in the range of 86.1–87.3 %. Among the prepared glasses, the $ZFPHo_{0.5}$ glass had the highest color purity (87.3 %).

Fig. 10 shows the normalized luminescence decay profiles of alkali

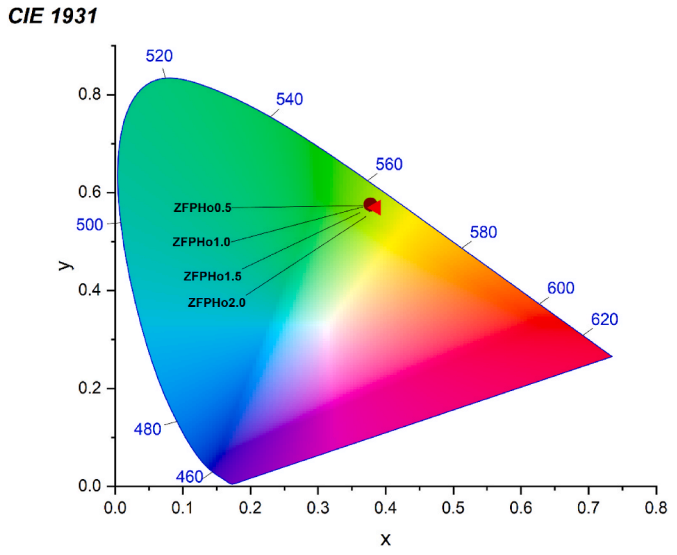

Fig. 9. CIE 1931 chromaticity colour diagram of different concentrations of Ho^{3+} ion-incorporated ZFP glasses excited at 450 nm. (For interpretation of the references to colour in this figure legend, the reader is referred to the Web version of this article.)

Table 7
CIE 1931 chromaticity colour coordinates (x, y), correlated colour temperatures (CCT, K), dominant wavelength nm and colour purity (%) of prepared Ho^{3+} ions-incorporated ZFP glasses.

Glass Sample	Colour Coordinates		Colour Coordinate Temperature	Dominant wavelength	Colour Purity
	x	y	CCT, (Kelvin)	nm	%
$ZFPHo_{0.5}$	0.383	0.574	4677	562.5	87.3
$ZFPHo_{1.0}$	0.382	0.573	4690	562.4	86.7
$ZFPHo_{1.5}$	0.377	0.576	4773	561.6	86.1
$ZFPHo_{2.0}$	0.386	0.569	4620	563.0	86.6

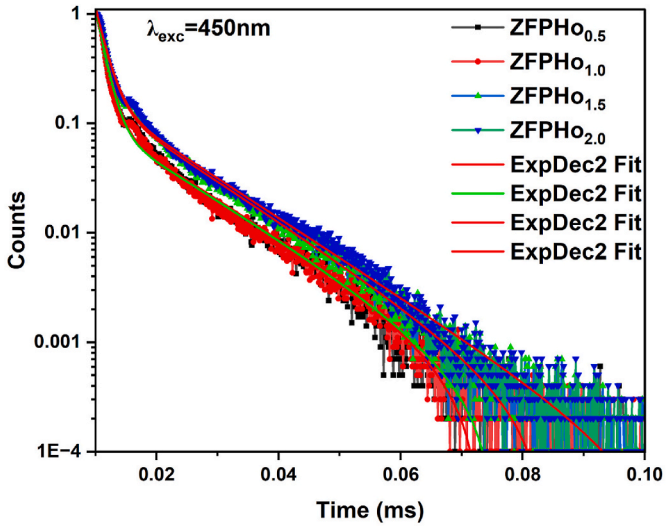

Fig. 10. Decay profiles for the $^5F_5 \rightarrow {}^5I_8$ emission transition of different concentrations of Ho^{3+} ions doped ZFP glasses at an excitation wavelength of 450 nm.

and alkaline ZFP glasses doped with different concentrations of Ho^{3+} ions for the $^5F_5 \rightarrow {}^5I_8$ transition at an excitation wavelength of 450 nm. The decay profiles of the studied glasses were well fitted with a double exponential decay fit, which represents the equation [54].

$$I(t) = A_0 + A_1\, exp\left(-t/\tau_1\right) + A_2\, exp\left(-t/\tau_2\right) \quad (7)$$

where $A_{0,1,2}$ are constants obtained from curve fitting, t is the time, and τ_1 and τ_2 are the decay lifetime values for the exponential components. The mean lifetimes (τ_{exp}) were obtained using the following equation from literature [54]:

$$\tau_{exp} = \frac{A_1\tau_1^2 + A_2\tau_2^2}{A_1\tau_1 + A_2\tau_2} \quad (8)$$

The obtained mean lifetimes (τ_{exp}) are 1.72, 1.70, 1.45 and 1.40 ms for $ZFPHo_{0.5}$, $ZFPHo_{1.0}$, $ZFPHo_{1.5}$, and $ZFPHo_{2.0}$, respectively. As the concentration of Ho^{3+} ions increases, the decay lifetime decreases. This phenomenon is mainly due to the shortened distances between neighbouring Ho^{3+} ions, which enhances the likelihood of interactions between ions and leads to concentration quenching (also known as self-quenching) [55]. Additionally, the higher concentration facilitates faster Ho^{3+}–Ho^{3+} energy transfer to quenching trap sites located near Ho^{3+} ions, further contributing to this effect [9].

4. Conclusions

Alkali and alkaline zinc fluorophosphate glasses doped with varying concentrations of Ho^{3+} ions were synthesized using a melt-quenching

technique. The amorphous nature of the glasses was confirmed by X-ray diffraction analysis. FTIR and Raman spectroscopies were used to determine the presence of functional groups and structural units. The optical absorption spectra exhibited ten peaks attributed to transitions from the ground state ($^5I_8$) to various excited states of Ho^{3+}. The Judd-Ofelt intensity parameters followed the trend $\Omega_2>\Omega_4>\Omega6$, indicating low symmetry and high covalency around Ho^{3+} ions. The emission spectra obtained under 450 nm excitation, revealed three main peaks corresponding to the $^5F_4\rightarrow{}^5I_8$, $^5F_5\rightarrow{}^5I_8$, and $^5F_4\rightarrow{}^5I_7$ transitions. The $^5F_5\rightarrow{}^5I_8$ transition exhibited the highest branching ratio (β_{exp}), stimulated emission cross section (σ_p), and bandwidth gain ($\sigma_p \times \Delta\lambda_{eff}$). Among the studied glasses, the $ZFPHo_{0.5}$ glass demonstrated superior optical performance with the highest branching ratio (96.30 %), stimulated emission cross-section (3.28×10^{-22} cm^2), and bandwidth gain (9.68×10^{-28} cm^3) for the $^5F_5\rightarrow{}^5I_8$ green emission transition, indicating its potential for efficient green laser output, surpassing glasses with higher Ho^{3+} concentrations, where concentration quenching diminishes efficiency. The $ZFPHo_{0.5}$ glass exhibited a color purity of 87.3 % with correlated color temperature (CCT) of 4773 K, approximating direct sunlight. The chromaticity coordinates position the emission in the yellowish-green region, which is optimal for visible-laser sources in display technologies, optical communications, and biomedical applications.

CRediT authorship contribution statement

B. Bujji Babu: Writing – original draft, Visualization, Investigation. **S. Vidya Sagar:** Software, Investigation, Formal analysis, Data curation. **K. Venkata Rao:** Writing – review & editing, Supervision. **C. Venkateswarlu:** Writing – review & editing, Validation, Investigation, Conceptualization. **N.V. Srihari:** Writing – review & editing, Validation, Formal analysis. **S.K. Annar:** Writing – review & editing, Validation.

Funding

This research did not receive any specific grants from funding agencies in the public, commercial, or not-for-profit sectors.

Declaration of competing interest

The authors declare that they have no known competing financial interests or personal relationships that could have appeared to influence the work reported in this paper.

Acknowledgements

Dr. K. Venkata Rao expresses gratitude to Professor Y. C. Ratnakaram, who serves in the Department of Physics at Sri Venkateshwara University in Tirupati, for his consistent assistance throughout this study.

Data availability

Data will be made available on request.

References

[1] R. Divina, P.E. Teresa, K. Marimuthu, Dy^{3+} ion as optical probe to study the luminescence behavior of Alkali lead bismuth borate glasses for w-LED application, J. Alloys Compd. 883 (2021) 160845, https://doi.org/10.1016/j.jallcom.2021.160845.

[2] M. Shoaib, I. Khan, K. Iskakova, M.M. Alam, G. Rooh, N. Chanthima, S. Kothan, I. Ullah, A. Ahad, J. Kaewkhao, Investigation of luminescence properties of Ho^{3+} doped barium, zinc and gadolinium based phosphate glasses, Optik 260 (2022) 169046, https://doi.org/10.1016/j.ijleo.2022.169046.

[3] K. Mariselvam, J. Liu, Green emission and laser properties of Ho^{3+} doped titano lead borate (TLB) glasses for colour display applications, J. Solid State Chem. 293 (2021) 121793, https://doi.org/10.1016/j.jssc.2020.121793.

[4] C. Zhang, L. Cao, C. Yun, Broadband 2.9 μm and 4.1 μm mid-infrared emission and energy transfer mechanisms in Ho^{3+}/Yb^{3+} co-doped tellurite glasses, J. Lumin. 257 (2023) 119764, https://doi.org/10.1016/j.jlumin.2023.119764.

[5] D. Möncke, H. Eckert, Review on the structural analysis of fluoride-phosphate and fluoro-phosphate glasses, J. Non-Cryst. Solids X 3 (2019) 100026, https://doi.org/10.1016/j.nocx.2019.100026.

[6] P. Meejitpaisan, S. Kaewjaeng, Y. Ruangthaweep, N. Sangwarantee, J. Kaewkhao, White light emission of gadolinium calcium phosphate oxide and oxyfluoride glasses doped with Dy^{3+}. https://doi.org/10.1016/j.matpr.2020.04.619, 2021.

[7] T. Duan, Y. Ji, W. Wang, Q. Zhang, Glass-forming region, structure, and properties of Ba(PO3)2- and Zn(PO3)2-based fluorophosphate glasses, J. Non-Cryst. Solids 634 (2024) 122977, https://doi.org/10.1016/j.jnoncrysol.2024.122977.

[8] Y. Tian, J. Zhang, X. Jing, S. Xu, Synthesis and spectroscopic characterization of $Ho^{3+}/Tm^{3+}/Pr^{3+}$ doped fluorophosphate glass, J. Mater. Sci. Mater. Electron. 24 (2013) 866–870, https://doi.org/10.1007/s10854-012-0837-z.

[9] V. Reddy Prasad, S. Damodaraiah, Y.C. Ratnakaram, Optical spectroscopy and luminescence properties of Ho^{3+} doped zinc fluorophosphate (ZFP) glasses for green luminescent device applications, Opt. Mater. 78 (2018) 63–71, https://doi.org/10.1016/j.optmat.2018.02.007.

[10] T.J. P, G. N, N. R, N. K, N.K.R. Nallabala, V.K. Kummara, K. S, P. Gadige, Optical and spectroscopic properties of Ho^{3+}-doped fluorophosphate glasses for visible lighting applications, Mater. Res. Bull. 124 (2020) 110753, https://doi.org/10.1016/j.materresbull.2019.110753.

[11] F. Baino, J. Marchi, R. Borges, E. Verné, Holmium-doped 58S glass-derived foam-like scaffolds, Mater. Lett. 341 (2023) 134256, https://doi.org/10.1016/j.matlet.2023.134256.

[12] P. Vani, G. Vinitha, R. Praveena, M. Durairaj, T.C. Sabari Girisun, N. Manikandan, Influence of holmium ions on the structural and optical properties of barium tellurite glasses, Opt. Mater. 136 (2023) 113438, https://doi.org/10.1016/j.optmat.2023.113438.

[13] J. Pisarska, K. Kowalska, M. Kuwik, J. Dorosz, M. Kochanowicz, J. Żmojda, D. Dorosz, W.A. Pisarski, Optical properties of titanate-germanate glasses containing Ho^{3+} ions, Mater. Res. Bull. 166 (2023) 112353, https://doi.org/10.1016/j.materresbull.2023.112353.

[14] Z.T. Naik, B.H. Rudramadevi, Photoluminescence properties of Ho^{3+} -doped fluoroborate optical glasses, Ferroelectrics Lett. 50 (2023) 20–29, https://doi.org/10.1080/07315171.2023.2189849.

[15] A.S. Alqarni, R. Hussin, S.K. Ghoshal, S.N. Alamri, Y.A. Yamusa, S.A. Jupri, Intense red and green luminescence from holmium activated zinc-sulfo-boro-phosphate glass: Judd-Ofelt evaluation, J. Alloys Compd. 808 (2019) 151706, https://doi.org/10.1016/j.jallcom.2019.151706.

[16] N. Wantana, E. Kaewnuam, N. Chanthima, H.J. Kim, J. Kaewkhao, Tuneable luminescence of Pr^{3+}-doped sodium aluminium gadolinium phosphate glasses for photonics applications, Optik 267 (2022) 169668, https://doi.org/10.1016/j.ijleo.2022.169668.

[17] B. Tioua, M.T. Soltani, A. Khechekhouche, L. Wondraczek, Physical properties and luminescence of highly stable erbium-doped antimony glasses for NIR broadband amplification, Opt Laser. Technol. 152 (2022) 108152, https://doi.org/10.1016/j.optlastec.2022.108152.

[18] V.A. Raj, A.J. D'Silva, K. Maheshvaran, M.M.A. Arasu, I.A. Rayappan, Concentration dependent Dy^{3+}- doped lithium fluoro borotellurophosphate glasses' structural and optical investigations for white light emission under UV excitation for solid-state lighting applications, Phys. B Condens. Matter 651 (2023) 414590, https://doi.org/10.1016/j.physb.2022.414590.

[19] S.B. Adamu, M.K. Halimah, K.T. Chan, F.D. Muhammad, S.N. Nazrin, R.A. Tafida, Eu^{3+} ions doped zinc borotellurite glass system for white light laser application: structural, physical, optical properties, and Judd-Ofelt theory, J. Lumin. 250 (2022) 119099, https://doi.org/10.1016/j.jlumin.2022.119099.

[20] P. Kaur, P. Kaur, J.S. Alzahrani, M.S. Al-Buriahi, T. Singh, Physical, structural and radiation absorption characteristics for some Eu^{3+} doped heavy metal oxide phosphate glasses, Optik 264 (2022) 169432, https://doi.org/10.1016/j.ijleo.2022.169432.

[21] Sk Mahamuda, F. Syed, ChB. Annapurna Devi, K. Swapna, M.V.V.K.S. Prasad, M. Venkateswarlu, A.S. Rao, Spectral characterization of Dy^{3+} ions doped phosphate glasses for yellow laser applications, J. Non-Cryst. Solids 555 (2021) 120538, https://doi.org/10.1016/j.jnoncrysol.2020.120538.

[22] F. Ahmadi, Z. Ebrahimpour, A. Asgari, S.K. Ghoshal, Insights into spectroscopic aspects of Er^{3+} doped sulfophosphate glass embedded with titania nanoparticles, Opt. Mater. 111 (2021) 110650, https://doi.org/10.1016/j.optmat.2020.110650.

[23] M. Shoaib, I. Khan, G. Rooh, S.M. Wabaidur, M.A. Islam, N. Chanthima, S. Kothan, I. Ullah, A. Ahad, J. Kaewkhao, Judd-Ofelt and luminescence properties of Pr^{3+} doped $ZnO\text{-}Gd_2O_3/GdF_3\text{-}BaO\text{-}P_2O_3$ glasses for visible and NIR applications, J. Lumin. 247 (2022) 118884, https://doi.org/10.1016/j.jlumin.2022.118884.

[24] S.A. Mohamed, Y.B. Saddeek, R. Elsaman, A.A. Showahy, T. Alharbi, Analysing the role of CoO in enhancing the radiation shielding properties of $ZnO–P_2O_5–Al_2O_3–PbO$ glasses using FTIR and ultrasound techniques, Radiat. Phys. Chem. 212 (2023) 111113, https://doi.org/10.1016/j.radphyschem.2023.111113.

[25] J. Biswas, S. Jana, Comparative studies on CIELab, thermal and optical characteristics of Dysprosium (Dy^{3+}) incorporated phospho-tellurite glasses for white light generation, Opt. Mater. 141 (2023), https://doi.org/10.1016/j.optmat.2023.113932.

[26] N. Ravi, G. Neelima, N.K.R. Nallabala, V.K. Kummara, R. Ravanamma, V.J. Reddy, M. Prasanth, K. Suresh, P. Babu, V. Venkatramu, Role of excitation wavelength and dopant concentration on white light tunability of dysprosium doped titania-fluorophosphate glasses, Opt. Mater. 111 (2021), https://doi.org/10.1016/j.optmat.2020.110593.

[27] M. Priya, M. Dhavamurthy, A.A. Suresh, M.M. Mohapatra, Luminescence and spectroscopic studies on Eu^{3+}-doped borate and boro-phosphate glasses for solid state optical devices, Opt. Mater. 142 (2023) 114007, https://doi.org/10.1016/j.optmat.2023.114007.
[28] S.A. Jupri, S.K. Ghoshal, M.F. Omar, K. Hamzah, N.N. Yusof, S.N. Syed Yaacob, S. K. Md Zain, I.M. Danmallam, Enhanced spectroscopic properties of holmium doped phosphate glass: role of Ag/TiO_2 nanoparticles embedment, J. Lumin. 252 (2022) 119380, https://doi.org/10.1016/j.jlumin.2022.119380.
[29] Z. Gao, J. Xing, Y. Luo, M. Liu, L. Yang, F. Shang, G. Chen, Optical temperature sensitivity, up-conversion luminescence and structure of $Ca_5(PO_4)_3F$: Yb^{3+}, Ho^{3+}, Tm^{3+} glass-ceramics, Opt. Commun. 527 (2023) 128951, https://doi.org/10.1016/j.optcom.2022.128951.
[30] M. Ennouri, L. Petit, H. Elhouichet, Investigations of the thermal, structural, and Near-IR emission properties of Ag containing fluorophosphate glasses and their crystallization process, Opt. Mater. 131 (2022) 112610, https://doi.org/10.1016/j.optmat.2022.112610.
[31] W.T. Carnall, P.R. Fields, K. Rajnak, Electronic energy levels in the trivalent lanthanide aquo ions. I. Pr^{3+}, Nd^{3+}, Pm^{3+}, Sm^{3+}, Dy^{3+}, Ho^{3+}, Er^{3+}, and Tm^{3+}, J. Chem. Phys. 49 (1968) https://doi.org/10.1063/1.1669893.
[32] B.R. Judd, Optical absorption intensities of rare-earth ions, Phys. Rev. 127 (1962) 750–761, https://doi.org/10.1103/PhysRev.127.750.
[33] G.S. Ofelt, Intensities of crystal spectra of rare-earth ions, J. Chem. Phys. 37 (1962) 511–520, https://doi.org/10.1063/1.1701366.
[34] B. Damdee, K. Kirdsiri, H.J. Kim, K. Yamanoi, N. Wongdamnern, P. Kidkhunthod, R. Rajaramakrishna, J. Kaewkhao, Physical and photoluminescence investigations of Eu^{3+} doped gadolinium borate scintillating glass, Radiat. Phys. Chem. 200 (2022) 110386, https://doi.org/10.1016/j.radphyschem.2022.110386.
[35] C. Görller-Walrand, K. Binnemans, Chapter 167 Spectral intensities of f-f transitions, in: Handbook on the Physics and Chemistry of Rare Earths, Elsevier, 1998, pp. 101–264, https://doi.org/10.1016/S0168-1273(98)25006-9.
[36] G. Lakshminarayana, A.N. Meza-Rocha, O. Soriano-Romero, E.F. Huerta, U. Caldiño, A. Lira, D.-E. Lee, J. Yoon, T. Park, Pr^{3+}-doped B_2O_3–Bi_2O_3–ZnO–NaF glasses comprising alkali/mixed alkali oxides for potential warm white light generation, blue laser, and E^-+S^-+C^-optical bands amplification applications, J. Mater. Res. Technol. 13 (2021) 2501–2526, https://doi.org/10.1016/j.jmrt.2021.06.037.
[37] G. Lakshminarayana, A.N. Meza-Rocha, O. Soriano-Romero, U. Caldiño, A. Lira, J. Yoon, Er^{3+}: B_2O_3-TeO_2-ZnO-PbF_2–M_2O/MF (M = Li, Na, and K) glasses: an inspection of structural, thermal, optical, chromatic, and near-infrared luminescence traits for displays and potential C-band amplification, J. Non-Cryst. Solids 622 (2023) 122660, https://doi.org/10.1016/j.jnoncrysol.2023.122660.
[38] M.K.K. Poojha, M. Vijayakumar, P. Matheswaran, E.S. Yousef, K. Marimuthu, Modifier's influence on spectral properties of dysprosium ions doped lead boro-telluro-phosphate glasses for white light applications, Opt. Laser Technol. 156 (2022) 108585, https://doi.org/10.1016/j.optlastec.2022.108585.
[39] N. Sooraj Hussain, N. Ali, A.G. Dias, M.A. Lopes, J.D. Santos, S. Buddhudu, Absorption and emission properties of Ho^{3+} doped lead–zinc–borate glasses, Thin Solid Films 515 (2006) 318–325, https://doi.org/10.1016/j.tsf.2005.12.085.
[40] M. Liu, J. Zhang, J. Zhang, Z. Zhang, G. Farrell, G. Brambilla, S. Wang, P. Wang, 2.4 μm fluorescence of holmium doped fluoroaluminate glasses, J. Lumin. 238 (2021) 118265, https://doi.org/10.1016/j.jlumin.2021.118265.
[41] Z. Zhou, C. Zhang, K. Han, T. Wu, D. Zhou, Broadband ~2 μm luminescence properties and energy transfer in Tm^{3+}/Ho^{3+} co-doped TeO_2–Al_2O_3–BaF_2 glass, Ceram. Int. 50 (2024) 35782–35790, https://doi.org/10.1016/j.ceramint.2024.06.399.
[42] T. Suhasini, B.C. Jamalaiah, T. Chengaiah, J. Suresh Kumar, L. Rama Moorthy, An investigation on visible luminescence of Ho^{3+} activated LBTAF glasses, Phys. B Condens. Matter 407 (2012) 523–527, https://doi.org/10.1016/j.physb.2011.11.029.
[43] F. Huang, G. Jiang, B. Chen, Y. Tian, J. Zhang, S. Xu, Effective 3.9 μm emission in fluorotellurate glass with Ho^{3+}: highly doping, J. Lumin. 265 (2024) 120203, https://doi.org/10.1016/j.jlumin.2023.120203.
[44] I. Abdullahi, S. Hashim, M.I. Sayyed, S.K. Ghoshal, Intense up-conversion luminescence from Dy^{3+}-doped multi-component telluroborate glass matrix: role of CuO nanoparticles embedment, Heliyon 9 (2023) e15906, https://doi.org/10.1016/j.heliyon.2023.e15906.
[45] S.K. Mohapatra, H.S. Maharana, S. Khan, S. Chakraborty, K. Annapurna, Ho^{3+}-activated calcium zinc silico-aluminate glass for 2 μm and 533 nm laser application, Mater. Today Commun. 37 (2023) 107477, https://doi.org/10.1016/j.mtcomm.2023.107477.
[46] K. Maheshwari, A.S. Rao, Photoluminescence downshifting studies of thermally stable Dy^{3+} ions doped phosphate glasses for photonic device applications, Opt. Mater. 129 (2022), https://doi.org/10.1016/j.optmat.2022.112518.
[47] A. Jose, T. Krishnapriya, J.R. Jose, C. Joseph, P.R. Biju, NIR photoluminescent characteristics of Nd^{3+} activated fluoroborosilicate glasses for laser material applications, Phys. B Condens. Matter 634 (2022) 413772, https://doi.org/10.1016/j.physb.2022.413772.
[48] B. Aull, H. Jenssen, Vibronic interactions in Nd:YAG resulting in nonreciprocity of absorption and stimulated emission cross sections, IEEE J. Quant. Electron. 18 (1982) 925–930, https://doi.org/10.1109/JQE.1982.1071611.
[49] W. Krupke, Induced-emission cross sections in neodymium laser glasses, IEEE J. Quant. Electron. 10 (1974) 450–457, https://doi.org/10.1109/JQE.1974.1068162.
[50] R. Rajaramakrishna, Y. Tariwong, N. Srisittipokakun, S. Kothan, J. Kaewkhao, 1.06 μm emission of neodymium doped P_2O_5+Al_2O_3+Li_2O+BaO+Gd_2O_3/GdF_3 glasses for solid-state NIR applications, J. Lumin. 257 (2023) 119650, https://doi.org/10.1016/j.jlumin.2022.119650.
[51] K. Kowalska, M. Kuwik, J. Pisarska, M. Leśniak, D. Dorosz, M. Kochanowicz, J. Żmojda, J. Dorosz, W.A. Pisarski, Influence of TiO2 concentration on near-infrared luminescence of Er^{3+} ions in barium gallo-germanate glasses, J. Mater. Res. Technol. 21 (2022) 4761–4772, https://doi.org/10.1016/j.jmrt.2022.11.081.
[52] M. Shoaib, I. Khan, N. Chanthima, A. Alhuthali, N. Intachai, S. Kothan, A. Ahad, I. Ullah, S. Khattak, G. Rooh, J. Kaewkhao, T. Ahmad, Photoluminescence analysis of Er^{3+}-ions Doped P_2O_5-Gd_2O_3/GdF_3-BaO-ZnO glass systems, J. Alloys Compd. 902 (2022) 163766, https://doi.org/10.1016/j.jallcom.2022.163766.
[53] S.V. Sagar, S. Babu, K.V. Rao, Emission spectroscopy of Sm^{3+} ion-activated zinc phosphate glass for reddish-orange lighting applications, J. Mater. Sci. Mater. Electron. 34 (2023) 2216, https://doi.org/10.1007/s10854-023-11608-y.
[54] J. Ding, C. Li, L. Xia, Y. Zhang, J. Li, Y. Zhou, A new $Nd^{3+}/Tm^{3+}/Ho^{3+}$ tri-doped tellurite glass for multifunctional applications, Mater. Res. Bull. 150 (2022) 111777, https://doi.org/10.1016/j.materresbull.2022.111777.
[55] L. Liu, J. Xing, F. Shang, G. Chen, Structure and up-conversion luminescence of Yb^{3+}/Ho^{3+} co-doped fluoroborate glasses, Opt. Commun. 490 (2021) 126944, https://doi.org/10.1016/j.optcom.2021.126944.